Progressive recruitment of distal MEC-4 channels determines touch response strength in *C. elegans*

Running title: Recruiting MeT channels for touch

Katta S.[1], Sanzeni A.[2], Vergassola M.[3], Goodman M.B.[1,4,*]

[1] Neuroscience Program, Stanford University, Stanford, CA 94025

[2] National Institute of Mental Health Intramural Program, National Institutes of Health, Bethesda, MD 20892

[3] Department of Physics, University of California, San Diego, La Jolla, CA 92093

[4] Molecular and Cellular Physiology, Stanford University, Stanford, CA 94025

*Correspondence to:

mbgoodman@stanford.edu

B-111 Beckman Center

279 Campus Dr

Stanford, CA 94305 USA

https://orcid.org/0000-0002-5810-1272

Summary

Through experiment and simulation, Katta, et al. reveal that pushing faster and deeper recruits more and more distant mechano-electrical transduction channels during touch. The net result is a dynamic receptive field whose size and shape depends on tissue mechanics, stimulus parameters, and channel distribution within sensory neurons.

Abstract

Touch deforms, or strains, the skin beyond the immediate point of contact. The spatiotemporal nature of the strain field induced by touch depends on the mechanical properties of the skin and the tissues below. Somatosensory neurons that sense touch often innervate large regions of skin and rely on a set of mechano-electrical transduction channels distributed within their dendrites to detect mechanical stimuli. We sought to understand how tissue mechanics shape touch-induced mechanical strain across the skin over time and how individual channels located in different regions of the strain field contribute to the overall touch response. We leveraged *C. elegans'* touch receptor neurons (TRNs) as a morphologically simple model and employed an integrated experimental-computational approach. Measuring mechanoreceptor currents (MRCs) in TRNs and performing biophysical modeling enabled us to dissect the mechanisms underlying the spatial and temporal dynamics that we observed. Consistent with the idea that strain is produced at a distance, we were able to elicit MRCs by delivering stimuli outside the anatomical receptive field. The amplitude and kinetics of the MRCs depended on both stimulus displacement and speed. Finally, we found that the main factor responsible for touch sensitivity is the recruitment of progressively more distant channels by stronger stimuli, rather than modulation of channel open probability. This principle may generalize to somatosensory neurons with more complex morphologies.

Introduction

Sensory receptor neurons are classified by their receptive fields -- the section of their sensory space in which a stimulus elicits a response, such as a spot in the visual field or a frequency in the ear. The receptive field of a somatosensory neuron is defined not only by its own spatial location, but also by the strain, or deformation, induced in the tissue by touch. Mechanical strain decreases with distance from the stimulus; the extent of the strain field and the speed of propagation depend on the intensity of the stimulus and the material properties of the neurons and skin being touched. With light and chemical stimuli, a single photon or ligand can only activate a single receptor protein at a time, even if many are in close proximity. With touch, a single indentation will simultaneously affect all eligible receptors that fall within the strain field, to a degree dependent on their distance from the point of stimulation. In the case of somatosensation, this means that multiple channels at spatially distinct sites within a neuron, or even multiple neurons, are liable to be activated to varying degrees by the same stimulus.

Intricate anatomical structures dedicated to mechanosensation are present in worms, flies, mice, cats, and humans. From the chordotonal organs and campaniform receptors of insects to Merkel cell touch domes and low-threshold mechanoreceptors arrayed around hair follicles in mammals, these structures place mechanosensitive proteins in specific arrangements around features of the skin or other mechanosensory organs (Katta et al., 2015). Increasing anatomical and functional data have provided insights into how these structures work. In many cases the complexity of skin has made it difficult to understand the strain field. While useful models have been created (Lesniak and Gerling, 2009; Quindlen et al., 2015; Quindlen-Hotek and Barocas, 2018; Sanzeni et al., 2018), few studies build on these models to generate an integrated understanding of how mechanical strain is detected by mechanosensitive proteins, including ion channels, distributed within somatosensory neurons.

Here, we probed how mechano-electrical transduction (MeT) channel distribution interacts with the strain field of a mechanical stimulus in a *C. elegans* touch receptor neuron (TRN). This system is a useful model because the factors governing the strain field are straightforward and the arrangement of channels is simple and well-characterized. Furthermore, we can directly measure the mechanoreceptor currents (MRCs). The six *C. elegans* TRNs (ALMR/L, PLMR/L, AVM, and PVM) extend long, straight neurites (Krieg et al., 2017) that are embedded in the epidermal cells that form the worm's skin or cuticle. External mechanical loads evoke MRCs that are carried by MEC-4-dependent MeT channels and are activated at both the onset and removal of mechanical stimuli (O'Hagan et al., 2005). The MEC-4 protein belongs to a large superfamily of non-voltage-gated ion channels conserved in animals but absent from microbes and plants (Katta et al., 2015). MEC-4 proteins localize to discrete puncta (Cueva et al., 2007; Emtage et al., 2004) that are arrayed along the entire length of TRN neurites, indicating that the MeTs responsible for touch in *C. elegans* are arranged in a single line. These anatomical properties make it easier to interpret how the geometry of the strain field depends on the size and speed of a given stimulus and determine which subset of MeT channels is likely to be affected by each stimulus.

Because MRC application depends more on indentation than it does on applied force (Eastwood et al., 2015), we developed and deployed a stimulator system enabling fast indentation and concurrent optical monitoring of probe movement. We used this system to measure MRCs evoked by mechanical stimuli delivered inside and outside of the apparent tactile receptive field of the ALM neuron and as a function of indentation depth and speed. By combining these experimental results with simulations (Sanzeni et al., 2018), we identified a biophysical mechanism linking indentation to MRCs. Specifically, we show that

MRC size and time-course depend primarily on the recruitment of distal channels in a model somatosensory neuron.

Materials and Methods

Nematode Strains

We used two strains of transgenic *C. elegans* nematodes: TU2769 *uIs31[mec-17p::gfp] III* (O'Hagan et al., 2005) for electrophysiology and GN865 *uIs31[mec-17p::GFP] III; kaIs12[col-19::GFP] ?* for imaging indentation. The *uIs31* transgene is a TRN-specific GFP marker that enables us to conduct *in vivo* recordings in TRNs. The *kaIs12* transgene encodes a GFP fusion to a collagen that labels cuticular annuli (Thein et al., 2003). We grew animals on OP50 and used well-fed subjects as late-L4 larvae or young adults.

Imaging Cuticle Deformation

We immobilized GN865 worms using 2% agarose pads with WormGlu (GluStitch); subjects were either left intact or dissected as described previously (Eastwood et al., 2015; O'Hagan et al., 2005). We used an Orca Flash 4.0LTv2 camera (Hamamatsu) controlled by µManager (Edelstein et al., 2010) on an upright microscope (E600FN, Nikon) under a 60X objective for imaging.

Electrophysiology

We recorded currents in the ALMR touch receptor neuron in TU2769 worms. The ALMR neuron is bilaterally symmetric to the previously studied ALML (Eastwood et al., 2015), which we could not stimulate mechanically due to the geometric constraints of this stimulator system. The extracellular solution contained (in mM): NaCl (145), KCl (5), $MgCl_2$ (5), $CaCl_2$ (1), and Na-HEPES (10), adjusted to a pH of 7.2 with NaOH. Before using the solution, we added 20mM of D-glucose, which brought the osmolarity to ~325mOsm. The intracellular solution contained (in mM): K-gluconate (125), KCl (18), NaCl (4), $MgCl_2$ (1), $CaCl_2$ (0.6), K-HEPES (10), and K_2EGTA (10), adjusted to a pH of 7.2 with KOH. Before use, we added 1mM of sulforhodamine 101 (Invitrogen) to help visualize whether the neuron was being successfully recorded.

We used an EPC-10 USB amplifier controlled by Patchmaster software (version 2x90.1, HEKA/Harvard Biosciences) to set the membrane voltage and control the mechanical stimulator. We corrected the membrane voltage for the liquid-junction potential (-14 mV) between the extracellular and intracellular solutions; we also corrected for errors that may have resulted from an imperfect space clamp based on stimulus distance, as described previously (Goodman et al., 1998; O'Hagan et al., 2005). Before digitizing the data at 10 kHz, we filtered the analog data at 2.9 kHz.

Mechanical Stimulation and Motion Detection

Some of the previous electrophysiological studies on *C. elegans* mechanoreceptor neurons have used open-loop systems with a piezoelectric bimorph (Árnadóttir et al., 2011; Bounoutas et al., 2009; Chen and Chalfie, 2015; Geffeney et al., 2011; O'Hagan et al., 2005) or a piezoelectric stack with no independent measurement of stimulator motion (Kang et al., 2010). We previously employed a slow

closed-loop system driven by a piezoelectric stack with a piezoresistive cantilever for force detection (Eastwood et al., 2015). Here, we used an open-loop system adapted from the piezoelectric stack system with a photodiode motion detector described by Peng and Ricci (2016) in their study on hair cells. This system enables faster stimulation than the force-clamp system and allows us to measure the time course of stimulation.

Using marine epoxy (Loctite), we attached an open-loop, piezoelectric stack actuator (PAS-005, ThorLabs, 20 µm travel) to a tungsten rod (L = 8 in.) to damp vibration. We mounted the rod-mounted actuator on a micromanipulator for positioning (MP-225, Sutter) and controlled the piezoelectric stack via an analog voltage output on a HEKA EPC-10 PLUS amplifier and Patchmaster software. We filtered this analog signal at 2.5 kHz or 5 kHz on an eight-pole Bessel filter (LPF-8, Warner Instruments) and used a high-voltage, high-current amplifier (Peng and Ricci, 2016) to achieve a signal between 0-75 V. The stack was biased with a starting offset of 3-4 µm, and the largest displacement we used was 3-4 µm short of the 20 µm total travel limit. This protocol ensured that stack motion was linearly related to the analog voltage signal.

Beads glued to force-clamp cantilevers create a defined and reproducible contact surface that is easy to model (Eastwood et al., 2015; Petzold et al., 2013). We adapted this technique for a system relying on glass, rather than silicon probes and for axial stimulus motion. We pulled and polished borosilicate glass pipettes (Sutter, BF150-86-10) to a tip diameter that was half or three-fourths of the diameter of the bead that we intended to use. We attached black polyethylene beads (20-24 µm diameter; BKPMS-1.2, Cospheric) to the glass pipettes using UV-curable glue (Loctite 352, Henkel). The bead-attached pipettes were then waxed to a 3D-printed acrylic pipette holder (custom design available from https://3dprint.nih.gov as Model ID 3DPX-010770) and epoxied to a steel tip (PAA001, ThorLabs) that was mounted on the piezo stack.

Step protocols had a 250 ms or 300 ms hold at the commanded indentation, and an inter-stimulus interval (ISI) of 1 s between sweeps. Trapezoidal protocols had a 300 ms hold and 2 s ISI. Sine protocols had a 1 s sine flanked by 300 ms steps, and 2 s ISI.

Photodiode Motion Detection

We adapted the system reported by Peng and Ricci (2016) for larger-scale movements by using the SPOT-2D segmented photodiode (OSI Optoelectronics) and a higher resistance in the differential amplifier circuit. The photodiode was mounted in an XY translator on top of a rotation stage (ST1XY-D, LCP02R, ThorLabs) such that the photodiode gap was aligned perpendicular to the direction of the probe motion. This apparatus was fixed above a secondary camera port on the microscope (Eclipse E600FN, Nikon) with no additional magnification.

Before making a gigaohm seal for patch clamp, we aligned the front edge of the bead under the 60X objective with the highest clearly visible edge of the worm's cuticle. After achieving whole-cell access, we moved the microscope to visually align the image of the bead with the outer edge of the photodiode. As the bead moved, the output from the photodiode circuit was read directly by Patchmaster, and we used this signal to check that resonance during steps and relative attenuation of sine amplitude at high frequencies were small.

At the end of each recording, we calibrated the image motion to actual motion. We drove the XY translator in steps of known distances in a direction that was opposite to the probe motion using a stepper motor actuator (ZFS-06, ThorLabs) controlled by Kinesis software (ThorLabs). We took these steps once with the probe at the edge of the worm and once with only the worm. Distances were measured relative to this starting position. The worm-only trace was subtracted from the probe+worm trace to obtain the relationship between the motion of the probe image and the known movement of the photodiode. We corrected stimulus traces from the recording using a piecewise cubic polynominal interpolation method ('pchip', MATLAB R2015b) of the mean voltage during calibration steps vs. the commanded photodiode motion at each step.

Data Analysis

We measured whole-cell capacitance and series resistance as previously described (Goodman et al., 1998). We conducted data analysis using MATLAB from Mathworks (data import and analysis functions are available online at: https://github.com/sammykatta/Matlab-PatchMaster/tree/vDynamics) and Igor Pro 6.37 (Wavemetrics).

Our analysis only included recordings with a holding current less than -10 pA at -60 mV and a series resistance less than 250 MΩ. As we did not change the voltage during these experiments, the voltage errors due to uncompensated series resistance were negligible, and therefore, we did not correct for these negligible errors. Where noted, we did correct for voltage attenuation due to space-clamp errors based on the distance from the cell body to the center of the stimulus. We calculated total charge, or the area under the MRC curve, from stimulus start to 150 ms after stimulus end, and subtracted the charge at baseline for an equivalent time period.

Simulations

For simulations, we used the model described in Sanzeni et al. (2018). Briefly, we made a finite element mechanical model of the worm as a pressurized thin-shelled cylinder. A three-state gating model of the channels allowed us to estimate the probabilities for individual channels to open. The total current flowing along the TRN is the sum of the currents flowing through the channels arrayed along the neuron that spans the length of the worm. Model parameters were fit according to the original dataset from (Eastwood et al., 2015) and not optimized for the data shown here. Only the intermediate internal pressure of 4 kPa was selected from previously tested values to better match the experimental data in this paper. For all of the simulations shown here, we have held this internal pressure constant. The stimulator was modeled as a rigid sphere with a 20 µm diameter.

Results

Mechanoreceptor currents in *C. elegans* TRNs are carried by an ensemble of MeT channels arrayed along the TRN neurite (Cueva et al., 2007; Emtage et al., 2004). For many other types of channels, an increase in macroscopic current is thought to reflect an increase in the open probability of a population of channels that receive the same stimulus at the same time. For these MeT channels, however, an increase in the macroscopic current cannot be interpreted primarily as an increase in open probability. As local indentation deforms tissue at distal sites (Fig. 1, A-C) in a manner that depends on indentation depth (Elmi et al., 2017; Sanzeni et al., 2018), stimulus intensity governs how many channels are

reachable by the stimulus and the probability that a given channel will open (Fig. 1 A). Similarly, we expect that stimulus speed influences the evolution of the strain field, thereby introducing an additional factor that affects the synchrony of MeT channel activation. As such, the spatial distribution of these MeT channels can affect how they respond to stimuli that vary across space and time.

MRC amplitude depends on stimulus depth and speed

To enable a thorough investigation of how indentation depth and speed influence activation of MeT channels in their native environment, we built a high-speed mechanical stimulator inspired by systems used to study hair cells in the auditory system (Peng and Ricci, 2016). While recording MRCs, we positioned this stimulator perpendicular to the worm's body and used the stimulator to push a stiff glass probe carrying a large (~22 µm) polyethylene bead into living, wild-type worms (Fig. 1 B and C). We recorded from ALM rather than PLM (O'Hagan et al., 2005). We pushed the bead perpendicularly rather than tangentially into the worm (Árnadóttir et al., 2011; Chen and Chalfie, 2015; Eastwood et al., 2015; O'Hagan et al., 2005) and used larger beads to deliver the mechanical stimulus (Eastwood et al., 2015). We also used high-speed stimulation. Unexpectedly, the peak MRCs we report here are about five-fold larger than previously reported (Fig. 1 E) and similar to those reported by Chen and Chalfie (2015).

Intrinsically larger responses in ALM versus PLM might account for some of the difference (Chen and Chalfie, 2015), but ALM currents measured with a force-clamped stimulus (Eastwood et al., 2015) were still significantly smaller than what we measured here (Fig. 1). Instead, we argue that the discrepancy in peak MRC size reflects differences in the stimulus paradigm or worm preparation between studies: the use of a larger bead to contact the animal's skin, high-speed stimulation, variations in body mechanics, or a combination of these factors. For a given indentation, our model (Sanzeni et al., 2018) predicts that larger beads and stiffer animals will generate larger strain fields, which would in turn affect more channels. In addition, the model predicts that current amplitude increases with stimulation speed at low speeds (Sanzeni et al., 2018). The indentation steps we applied here are at least an order of magnitude faster than those of the FALCON system or those previously modeled (Eastwood et al., 2015; Sanzeni et al., 2018). Lastly, dissection of cell bodies for recording creates variation in body stiffness that affects peak current amplitude (Sanzeni et al., 2018), but this is unlikely to account for the ten-fold change in mean MRC amplitude (Fig. 1 E). Based on these considerations, we infer that the bead size and stimulus speed are the dominant factors that account for the larger currents we have reported here.

In addition to these factors, indentation depth also affects peak current amplitude and total charge transferred (Fig. 2, A and B, left). Increasing the indentation depth has two effects, as demonstrated in our computational model linking tissue mechanics to MeT-channel activation in living animals (Sanzeni et al., 2018). The first effect is expansion of the strain field, which increases the number of channels available for activation. The second effect is an increase in the probability that a given MeT channel is activated. This model also shows that the channels closest to the point of stimulation, where the deformation is greatest, are more likely to open than distant channels (Fig. S1). These two effects combine to determine MRC peak amplitude as well as the total charge transferred and result in non-linear current-indentation curves (Fig. 2, A and B, right).

Although we expect variations in body stiffness and internal pressure due to the dissection procedure (Eastwood et al., 2015), these parameters are outside of experimental control. To circumvent this

technical limitation, we used simulations to systematically explore the influence of variations in pressure (Fig. 2, A and B, right). We used the model of Sanzeni, *et al.* (2018): with the exception of internal pressure, the free parameters of the simulation were derived by fitting a dataset collected with a different stimulation system (Eastwood et al., 2015). Higher internal pressures correspond to stiffer animals and lower pressures correspond to softer ones. The simulated current amplitude for a 10 µm indentation is higher in stiff animals compared to softer ones (Fig. 2 A). Our simulations used the original parameters from that dataset and an internal pressure of 4 kPa, which reflects an intermediate stiffness.

In all prior studies, current-indentation curves for MeT channels have been treated as a saturating function of stimulus size. Our experimental and computational results suggest that such a treatment neglects the influence of tissue mechanics as well as the de-localized nature of MeT channels. Furthermore, our results show that the shape of the current-indentation curve depends on factors extrinsic to the MeT channels themselves.

Using the Sanzeni, *et al.* (2018) model, we further examined the effect of displacement on current by separating the effect of indentation on open probability from the effect of indentation on increased channel recruitment via an expansion of the strain field. In this model, the open probability of each channel depends on its location relative to the stimulus. The simulation assumed that each fully open single channel carried -1.6 pA and channels could enter a sub-conducting state by carrying half of the single-channel current. These assumptions are consistent with *in vivo* estimates of single-channel amplitude (O'Hagan et al., 2005) and single-channel recordings of MEC-4-dependent channels (Brown et al., 2008). We used the mean peak current for each channel as a concise method of describing the single channel response regardless of the number of sub-conductance states used in the model. Regardless of whether we only included channels that reach a fully open state or added in sub-conducting channels above a threshold of -0.16 pA, we observed that the mean current per channel rose with small displacements, but then held steady (Fig. 2 C). In contrast, the number of open channels continued to increase with increased displacement (Fig. 2 D). The jump in the number of channels around 5µm displacement is due to a non-linear recruitment of a population of distant channels with low open probability (Fig. S1), which in turn decreases the average current per channel (Fig. 2 C). Collectively, these results suggest that channel recruitment, rather than changes in open probability, dominate the current-indentation relationship. The inclusion of sub-conducting channels more closely reflects the behavior of both current and charge. As such, all subsequent plots of this type reflect the O+SC condition.

MeT channels are activated by distant stimuli

Our results suggest that indentation at one point along the body actually affects multiple channels along the neurite. Thus, we expect that MRC amplitude depends on the overlap between the strain field and the neurite (Fig. 3 A). We explored this concept experimentally by holding the stimulus size constant and varying the distance between the ALM cell body and the stimulator in both the anterior and posterior directions (Fig. 3 B). For recordings obtained while stimulating anterior to the cell body, we corrected for errors arising from the fact that the TRNs are not isopotential (Materials and Methods). Although we did not detect a systematic relationship between current amplitude and distance from the cell body in the anterior direction (Fig. 3 B, blue), the high variation in current amplitudes across individual recordings

could mask such a relationship. Additional experiments involving measurements at several positions during a single recording may resolve this uncertainty.

There are no channels from ALM posterior to its cell body. Despite this fact, we found that stimulating up to 100 µm posterior to the ALM cell body successfully evoked MRCs (Fig. 3 B). On average, these currents had smaller amplitudes than currents elicited by stimuli of an equivalent magnitude anterior to the cell body (Fig. 3, B and C). Although the variation in current amplitude was lower than the variation we observed for anterior stimulation, there was no obvious relationship between current amplitude and distance from the cell body in the posterior direction. At larger distances, we did not observe detectable currents even with large displacements (n = 4).

Consistent with the reduced overlap between the strain field and the neurite for posterior stimulation, larger displacements were necessary for eliciting currents under this condition (Figs. 3 C and 4, A and B). Peak current-displacement curves were shifted to the right relative to curves observed for anterior stimulation such that the posterior stimulation only evoked consistently detectable MRCs for indentations larger than 4 µm. Simulations captured this shift in peak current-indentation curves (Fig. 4 A, right) and suggested that the size of the shift is proportional to the distance from the cell body. We also plotted the total charge—the area under the MRC curve—against displacement to account for differences in the timing of channel opening. This reduced the difference in operating range in our experimental data (Fig. 4b, left), but not in the simulations (Fig. 4 B, right). This suggests that channels activated during posterior stimulation are activated in a less synchronous manner than channels activated during anterior stimulation. For both measures, larger stimuli are necessary for activating channels in the simulations.

Given the discrepancy between peak current and total charge, we looked at the how the activation and decay rates varied with displacement in anterior and posterior recordings. Passive conduction over a long distance can broaden the time course of electrical events measured at the cell body (Bekkers and Stevens, 1996; Rall, 1967). Therefore, we limited this analysis to stimuli within 90 µm of the cell body—less than the average length constant $\lambda = 96 \pm 3$ µm (mean ± s.e.m., $n = 83$) calculated for our recordings—for both anterior and posterior recordings.

We estimated activation rates by measuring the time required for the current to rise to half the peak value from the start of the stimulus, and decay rates from the time to peak to when the current dropped to half the peak value. Activation rate increased with stimulus size and were similar for anterior and posterior stimulation (Fig. 4 C). We failed to detect any difference in latency. The decay rate for anterior—but not posterior—stimulation increased slowly with displacement (Fig. 4 D). This observation is consistent with space-clamp error for channels beyond the point of stimulation: larger stimuli affect channels that are much further away from the cell body and the contribution of these channels to the total current measured at the cell body is slowed and decreased by passive conduction. Indeed, when we included recordings in which the stimulator was placed even further anterior to the cell body, we found that both the activation and decay were slower (data not shown). Channels activated by posterior stimulation are located near the cell body, where this error is low, but their position at the edge of the strain field means they are activated only weakly. The simulation does not consider space clamp error, but predicts faster decay with posterior stimulation because tissue experiencing low strain only needs to move a short distance to relax. Although the smaller shift of total charge is not explained by this finding, simulations of activation and decay rates agree qualitatively with the experimental results in at least one

other way: the further posterior the stimulator is placed, the larger the displacement required to reach any channels in the neurite (Fig. 4 C and D, right). The simulation predicts slower activation times for posterior stimulation because strain takes longer to reach distant channels than proximal channels. However, we could not clearly detect such a difference in our experiments with this fast step protocol.

As noted above, the macroscopic currents we record depend on 1) stimulus-dependent changes in a channel's open probability; and 2) the number of channels exposed to each stimulus. Using average single-channel current as a proxy for open probability, our simulations predict that channel open probability saturates at smaller displacements for anterior stimuli than for posterior stimuli (Fig. 4 E). Also, the fact that larger stimuli reach more channels than smaller stimuli is the dominant factor controlling peak current-displacement curves for both anterior and posterior stimuli (Fig. 4 A).

MRC size and activation rate depend on stimulus speed and direction

The peak amplitude of MRCs in *C. elegans* TRNs increases with the speed of indentation (Fig. 5 A, 6 A left). This could reflect speed-dependent activation of individual channels. It could also reflect a speed-dependent increase in synchrony, or in-phase activation, of a population of channels. To differentiate between these possibilities, we analyzed peak current and charge (the area under the MRC curve) across a wide range of speeds and with fine resolution. Unlike peak MRC size, charge accounts for all channel openings regardless of timing. It follows, therefore, that if the speed-dependence of peak MRC amplitude were entirely due to variations in the phase of channel opening, then charge would be independent of speed. In contrast to this prediction, we found that charge was also speed dependent in both experiments and simulations (Fig. 6 B). Collectively, these findings indicate that variations in the phase of channel activation are not sufficient to account for the speed dependence of MRC generation.

In contrast to displacement sensitivity, measured current and charge appear to saturate at high speed and simulated current and charge clearly saturate at speeds above 1,000 µm/s (Fig. 6 A, B left). This finding suggests that indentation depth governs the number of channels eligible for recruitment. To estimate the relative contributions of channel recruitment and gating to speed dependence, we turned to simulations, which predicted a similar dependence on speed (Fig. 6 A-D right). We found that both peak channel current and the number of open channels saturate at high speeds (Fig. 6 E, F) and that the number of open channels increases strongly with stimulus speed (Fig. 6 F).

The saturating number of channels depends on the value of x_h, a model parameter controlling the force needed to activate a single channel, with smaller parameter values recruiting more channels (Fig. 6 F). Thus, for a fixed final displacement there seems to be a maximal number of channels that can be opened and this number is expected to be inversely proportional to the force needed to activate single channels. For a given x_h, the model suggests that the increase in the number of open channels with speed results from strain changing faster and generating larger forces on the channels.

Both 'on' and 'off' mechanoreceptor currents increase in size with stimulus speed (Figs. 5 A-C and 6 A and B, left), but to different extents. With large indentations at low speeds, 'off' MRCs have a larger peak current than 'on' MRCs, but at high speeds, the ratio reverses (Fig. 5 D). Above, we argued that synchrony or phase differences in channel activation do not fully account for speed-dependence generally. However, we explored the possibility that this was a significant factor in the asymmetry we

observed in peak current amplitudes between ‘on’ and ‘off’ responses by plotting the ratio of ‘off’ to ‘on’ charge against stimulus speed. We found that ‘off’ responses were consistently smaller than ‘on’ responses, but no evidence for speed dependence in this ratio (Fig. 5 E).

‘On’ currents activate slowly at slow speeds, while ‘off’ currents activate rapidly and vary less with stimulus speed in both experimental and simulated data (Fig. 6 C). The simulation additionally predicts that recruiting more channels by decreasing x_h increases the asymmetry in activation (Fig. 6 C, right). This is not true for the decay rate, however. Both ‘on’ and ‘off’ MRCs seem to decay at a relatively constant rate regardless of stimulus speed (Fig. 6 D). This suggests that activation depends on stimulus speed, while decay depends on tissue relaxation. Intuitively, we might expect channels to be more likely to be opened in-phase during 'off' stimuli because all channels affected by the deformation will start moving once the stimulator moves. In contrast, during slow ‘on’ stimuli, channels closer to the stimulator will be affected before the deformation reaches further channels, resulting in out-of-phase opening and slower MRC activation. This is supported by the observation that activation of ‘on’ MRCs appears to be faster at high speeds (Figs. 5 B and 6 C). The activation rate of ‘off’ currents is much less dependent on stimulus speed (Figs. 5 C and 6 C), but the amplitude of ‘off’ currents still increases with speed despite this greater synchrony (Fig. 6 A), suggesting there exists another mechanism for speed dependence.

Sinusoidal stimuli evoke steady MRCs in a frequency-dependent manner

While our stimuli thus far have been simple steps or trapezoids, the stimuli a worm encounters in the wild or even in the laboratory (Nekimken et al., 2017) involve complex signals with a variety of frequencies. Prior work shows that the TRNs seem poised to respond to variable signals given that calcium responses to sinusoidal "buzz" stimuli are also much stronger than those evoked by simple steps (Fehlauer et al., 2018; Suzuki et al., 2003). Therefore, we systematically examined the frequency response to sinusoidal mechanical stimuli at frequencies ranging from 10 Hz to 1kHz. The representative traces in Fig. 7 A show both the signal from the photodiode measuring the bead motion as well as the currents evoked by this stimulation. We see little evidence of adaptation. However, there does seem to be some adaptation in current between the beginning of the sine and the end, which may be partially attributed to the stimulus design, with the sudden onset and offset of the sine acting as a step. The responses to a step 300 ms before and after a 1 s-sinusoid show no more than 10-15% attenuation. This result starkly contrasts with studies on Piezo1 and Piezo2 channels, which show persistent adaptation just 10 s after sinusoidal stimulation (Lewis et al., 2017).

In agreement with our previously reported experimental and simulation results (Eastwood et al., 2015; Sanzeni et al., 2018), the expanded traces show that inward currents occur at twice the frequency of the stimulus (Fig. 7 B), especially at frequencies below 500 Hz. This suggests an alternation between 'on' and 'off' responses. At higher frequencies (1 kHz, not shown), we saw substantial attenuation in the amplitude of the sine stimulus, due to the bandwidth of our stimulation system (Methods). We next examined the power spectral density of the stimulus and the MRC response. We found that MRCs have roughly equal power at 1x and 2x the stimulus frequency (Fig. 7 C), whereas the spectrum of the stimulator shows a larger peak at the stimulus frequency and a smaller one at its 2x harmonic. The relative power of the 2x peak in the MRC response decreases slightly at higher frequencies, which is

reflected in the decreasing asymmetry between subsequent ('on' vs. 'off') peaks (Fig. 7 B). This finding demonstrates that the neuron's response to stimulation is non-linear.

The average steady-state current continues to increase with frequency (Fig. 7 A, D). Although the experimental data are shifted to the right relative to the predictions of the model with the previously set parameters (τ = 2.9 ms), both traces show the tissue acting as a high-pass filter (Fig. 7 D). This is consistent with TRNs being relatively insensitive to slowly varying stimuli and thus ignoring self-motion. By contrast, the amplitude of the current around the steady-state mean, as measured by the root mean square (RMS) of the response at steady state, shows band-pass behavior (Fig. 7 E). Again, the peak of the experimental curve is shifted to higher frequencies than the model predicts with the previous parameters (dashed line). The band-pass behavior in Fig. 7 E can be understood as being due to the fact that channels do not have time to transition to lower-conductance states during high-frequency stimulation. Because the channels are held in an open or sub-conducting state, their contribution to the RMS noise declines.

We hypothesized that the simulated results were shifted to the left because channels were not able to close adequately between the rise and fall of the sine stimulus. To test this possibility, we shortened the time required for the elastic filament to relax to baseline (τ), which allowed us to better match the peak RMS (Fig. 7 E). However, this change also shifted the steady-state current too far to the right. These observations suggest that additional modifications to model parameters could fine-tune the mechanical filter that links touch sensation to MeT channel activation.

Single channel activation is a function of position and stimulus intensity

Our model allows us to explore spatial and temporal dynamics not only at the level of macroscopic currents, but also at the individual channel level. We selected four channels at varying distances from one realization of the simulation, and calculated the expected ‘on’ and ‘off’ responses to various displacements, speeds, and sine frequencies. Our goal was to examine how MRC dynamics vary along the length of the neurite and as a function of stimulus type.

The simulated channel current reflects the weighted probability that a channel at this location is in an open or sub-conducting state. The maximal current possible is -1.6 pA, which is the value calculated from the measured single-channel conductance (Brown et al., 2007) and our recording conditions. Channels that are more distant from the center of the stimulator only begin to respond with large stimulus displacements (Fig. 8 A, highlighted). Channels directly under the stimulus (A, rightmost column) reach a fully open state even with small displacements; with larger displacements, the open probability remains high for longer periods of time even when the step takes the same amount of time. The total current predicted by the simulation (Fig. 8 A, left panel) is smaller than what we observed at high speeds, which could reflect a difference in channel distribution. Channels in the model are distributed based on the previously measured log-normal distribution (Cueva et al., 2007).

When we held displacement constant and varied the speed, we found that ‘on’ and ‘off’ currents activate faster at higher speeds through a combination of synchrony and increasing open probability. Channels distant from the stimulus take longer to receive and respond to ‘on’ stimuli at slow speeds (Fig. 8 B, highlighted). Channels at the point of stimulation (B, rightmost column) behave the opposite:

although the 'off' current initially rises like the 'on' current, it then slows and takes longer to reach the peak. Intermediate channels (B, second to right column) open both faster and more fully with increased speed. This dependence on channel distance is inherited from the underlying strain dynamics and explains the predicted slow offset activation times (Fig. 6 C), which depend more strongly on the most proximal channels, and reflects the fact that the time course of strain rate depends on distance from the stimulus.

The model nicely captures the increasing steady-state current that occurs when we increase the sine frequency. However, the fluctuations in the current (measured earlier as the RMS) are larger experimentally (Fig. 8 C, left panels). In both the observed and simulated data, the relative amplitudes of the peaks at 2x the stimulus frequency also decrease with frequency. Thus, the 'off' response seems weaker. The open probability for channels near the stimulus remains more constant at higher frequencies (Fig. 8 C, highlighted column). The intensity of the stimulus reaching the channel is attenuated in distal channels, as seen by their lack of response to smaller or slower indentations (Fig. 8 A and B), which contributes to the decrease in RMS.

Discussion

Using experiments and simulations, we develop a mechanistic understanding of how touch is transformed into depolarizing currents in touch receptor neurons. The picture emerging from this work is that touch sensitivity and filtering depend on tissue mechanics as well as the distribution of ion channels within sensory neurons. In particular, our results show that both the depth and speed of indentation affect the amplitude and time course of MRCs. Current-indentation curves do not saturate and display inflections that vary with internal pressure. By contrast, when we hold displacement constant, both the peak MRC-speed and charge-speed curves saturate at high speeds. The increase in peak current with speed occurs partially due to increased synchrony of channel openings with faster stimuli. Yet the total charge—which reflects all channel openings during the MRC—also increases with stimulus speed, suggesting that even without the effect of synchrony, MRCs depend on stimulus speed. This idea is also supported by the fact that 'off' responses, which have more synchronous activation, show a similar dependence on stimulus speed. Collectively, these observations indicate that activating MRCs in their native environment depends on tissue mechanics and dynamics as well as on the intrinsic mechanosensitivity of the MeT channels that carry the currents.

Two mechanisms govern MRC amplitude

Both displacement and speed affect MRCs through a combination of two mechanisms: 1) recruiting individual channels; and 2) modulating the open probability for each channel. In general, the macroscopic current for ion channels $I = i*N*P_o$ depends on the single-channel current $i = \gamma\ (V_m - E_{rev})$, the number of channels available to be activated N, and the average open probability P_o.

In many systems, we can justifiably assume that N remains constant regardless of stimulus intensity and tends to change only when channels become inactivated. We can also assume that while P_o varies with stimulus intensity, it remains consistent across channels. For touch sensation, neither of these assumptions hold true. Both our experimental and simulated data are consistent with the idea that

larger displacements recruit increasingly distant channels by expanding the strain field. We previously showed that a displacement of a given magnitude elicits a larger response when the displacement begins from a pre-indented position (Sanzeni et al., 2018); this may occur due to a combination of wider recruitment and increased synchrony of activation. When we positioned the stimulus posterior to all channels, the curve was shifted to the right (larger displacements) because we began to observe responses only once the displacement was large enough for the mechanical strain to reach the nearest channels (Figs. 3, 4, and 8). Our model also shows that both larger displacements and faster speeds increase the number of channels that fall within the indentation-induced strain field, which makes them susceptible to opening (Figs. 2 D and 6 F). Increasing either displacement or speed can increase the probability that a channel will be in a sub-conducting or open state. However, these probabilities vary for each channel and depend on the channel's distance from the stimulus (Fig. 8).

We uncovered further evidence for the involvement of two mechanisms by discovering that our experimental and simulated relationships between the stimulus speed and current were not well fit by a saturating Boltzmann function, as might be expected if open probability were the only factor. The total charge, in fact, appeared to have two or more distinct steps that may reflect differences in the relative contributions of increased open probability and recruitment (Fig. 6 B). Although we held the final displacement constant across speeds, the rate of strain, which determines the magnitude of the force acting on the channels in the model, increases with faster stimulation. Even if *N* remains constant across all speeds, the distribution of open probabilities likely changes with curvature and strain near the stimulator. Curvature and strain, in turn, depend on body mechanics. This distribution might also include the effect of sub-conductance states previously observed in channels that are heterologously expressed and constitutively open (Brown et al., 2008, 2007). Our model predicts that channels that are farther away from the stimulus are more likely to be in a sub-conducting rather than a fully open state. Moreover, increasing the speed might increase the proportion of open to sub-conducting channels in a non-linear manner.

MRC kinetics and on/off asymmetry depend on channel recruitment

The model supports the idea that channels located farther away from the center of stimulation are recruited and opened later. However, the difference in timing is noticeable only at slower speeds (Fig. 8 B), when changes in displacement can be spread across time. Distant channels experience increases in strain with a more diffuse and delayed time course because displacement is not instantaneous. The rate at which strain changes for distal channels can be high only when the displacement is large enough to reach them, which occurs late in an 'on' ramp or early in an 'off' ramp. Proximal channels, conversely, experience the greatest changes in strain at small displacements, where the curvature changes most drastically. As the proportion of distal to proximal channels increases with greater recruitment, the overall time course shifts toward the distal temporal profile, with slow 'on' activation and fast 'off' activation, creating asymmetry in MRC kinetics.

Similar to intact mammalian Pacinian corpuscles (Mendelson and Loewenstein, 1964), the DEG/ENaC/ASIC channels in *C. elegans* TRNs respond with nearly symmetrical depolarizing currents at both the onset and offset of an indentation step (Árnadóttir et al., 2011; Eastwood et al., 2015; O'Hagan et al., 2005). In this study, we also observed nearly identical responses at stimulus speeds around 1mm/s, but varying the speed varied the asymmetry between peak 'on' and 'off' currents. The

significant increase in activation time and the relative invariance of total charge across speeds suggest that the high 'off'/'on' ratio at slow speeds is due to a change in synchrony (Fig. 6). Many MeT channels show asymmetrical responses to the onset and offset of a stimulus. This is usually because they inactivate (Lewis et al., 2017), or because these channels are part of asymmetrical structures that provide directional force to the channels (Katta et al., 2015). Our current and previous models assume that individual channels receive symmetrical forces at the onset and offset of stimuli (Eastwood et al., 2015; Sanzeni et al., 2018). Here, we show that asymmetry is dynamic and is produced at the population level by stimulus-dependent, spatiotemporal recruitment of channels at different locations.

Implications for understanding touch in vivo

Pacinian corpuscles show the same type of rapidly adapting response when intact, but are much more slowly adapting when de-lamellated -- the high-pass side of the filter seems to be a result of mechanics (Loewenstein and Mendelson, 1965; Loewenstein and Skalak, 1966). In addition, Pacinian corpuscles seem to require the lamellae to sustain the 'off' response. Although *C. elegans* TRNs differ in their anatomical structure, the mechanics of the body as a fluid-filled shell creates a similar mechanical filter that theoretically leads to adaptation. Furthermore, the congruence between model dynamics and experimental dynamics lends credence to the model. We can pursue this line of research by directly measuring the distribution of strain throughout the body and along the TRN neurite. How would these MeT channels respond if we stimulated them in cultured neurons without body mechanics filtering the force? Would the channels still show the same rapidly-adapting behavior and responses to both stimulus onset and offset? The results presented here and in (Sanzeni et al., 2018) indicate that tissue mechanics play a crucial role in shaping the response to touch. Thus, we would not expect to recapitulate the dependence on indentation depth and speed *in vitro* that is found *in vivo*.

Although the model reflects and explains many of the dynamics we see experimentally, there are still differences that hint at biological mechanisms as yet unaccounted for by the model. While many of these discrepancies can be resolved by better matching existing parameters to the recordings, a few qualitative observations may require more consideration. For large displacements, the total charge for 'on' responses is consistently higher than the 'off' response at all speeds, which might suggest either a mechanism of inactivation at the level of the channel, or an irreversible dismantling of the molecules involved in transmitting force. The rightward shift in frequency dependence and the presence of responses to distal posterior stimulation are also findings that reflect a discrepancy between the model and the experimental data. Perhaps the distribution of MeT channels varies along the length of the neurite, with a greater concentration near the cell body. Alternatively, this discrepancy could be due to extracellular collagen networks or cytoskeletal structures like microtubules, which could render the neuron stiffer than the surrounding tissue and direct force down the neurite. Luckily, *C. elegans* also provides many genetic tools for perturbing these elements and assessing their contributions to the spatial and temporal dynamics of mechanoreceptor responses. Now we can explore the effects of mutations in skin and neuronal proteins on mechano-electrical transduction within the context of a larger, overarching biophysical model.

Acknowledgements

We thank Z. Liao for superb technical support and animal husbandry; V. Vásquez, A. Peng, F. Loizeau and A. R. Ricci for assistance with the design, fabrication and testing of the mechanical stimulator and optical displacement sensor; and D. Ó Maoiléidigh and members of the Goodman laboratory for comments on the manuscript. Research supported by a Ruth L. Kirschstein fellowship (F31-NS-093825) to SK and NIH grants (R01-NS-047715; R35-NS-105092) to MBG.

Author Contributions

All authors contributed to conceptualization, methodology, and revision of the final manuscript. Collection and analysis of experimental data were performed by SK while simulations were carried out by AS, with supervision by MBG and MV, respectively. SK created the visualizations and the initial draft.

References

Árnadóttir, J., O'Hagan, R., Chen, Y., Goodman, M.B., Chalfie, M., 2011. The DEG/ENaC Protein MEC-10 Regulates the Transduction Channel Complex in Caenorhabditis elegans Touch Receptor Neurons. J. Neurosci. 31, 12695–12704. https://doi.org/10.1523/JNEUROSCI.4580-10.2011

Bekkers, J.M., Stevens, C.F., 1996. Cable properties of cultured hippocampal neurons determined from sucrose-evoked miniature EPSCs. J. Neurophysiol. 75, 1250–1255. https://doi.org/10.1152/jn.1996.75.3.1250

Bounoutas, A., O'Hagan, R., Chalfie, M., 2009. The Multipurpose 15-Protofilament Microtubules in C. elegans Have Specific Roles in Mechanosensation. Curr. Biol. 19, 1362–1367. https://doi.org/10.1016/j.cub.2009.06.036

Brown, A.L., Fernandez-Illescas, S.M., Liao, Z., Goodman, M.B., 2007. Gain-of-Function Mutations in the MEC-4 DEG/ENaC Sensory Mechanotransduction Channel Alter Gating and Drug Blockade. J. Gen. Physiol. 129, 161–173. https://doi.org/10.1085/jgp.200609672

Brown, A.L., Liao, Z., Goodman, M.B., 2008. MEC-2 and MEC-6 in the Caenorhabditis elegans Sensory Mechanotransduction Complex: Auxiliary Subunits that Enable Channel Activity. J. Gen. Physiol. 131, 605–616. https://doi.org/10.1085/jgp.200709910

Chen, X., Chalfie, M., 2015. Regulation of Mechanosensation in C. elegans through Ubiquitination of the MEC-4 Mechanotransduction Channel. J. Neurosci. 35, 2200–2212. https://doi.org/10.1523/JNEUROSCI.4082-14.2015

Cueva, J.G., Mulholland, A., Goodman, M.B., 2007. Nanoscale Organization of the MEC-4 DEG/ENaC Sensory Mechanotransduction Channel in Caenorhabditis elegans Touch Receptor Neurons. J. Neurosci. 27, 14089–14098. https://doi.org/10.1523/JNEUROSCI.4179-07.2007

Eastwood, A.L., Sanzeni, A., Petzold, B.C., Park, S.-J., Vergassola, M., Pruitt, B.L., Goodman, M.B., 2015. Tissue mechanics govern the rapidly adapting and symmetrical response to touch. Proc. Natl. Acad. Sci. 112, E6955–E6963. https://doi.org/10.1073/pnas.1514138112

Edelstein, A., Amodaj, N., Hoover, K., Vale, R., Stuurman, N., 2010. Computer Control of Microscopes Using µManager. Curr. Protoc. Mol. Biol. 92, 14.20.1-14.20.17. https://doi.org/10.1002/0471142727.mb1420s92

Elmi, M., Pawar, V.M., Shaw, M., Wong, D., Zhan, H., Srinivasan, M.A., 2017. Determining the biomechanics of touch sensation in C. elegans. Sci. Rep. 7, 12329. https://doi.org/10.1038/s41598-017-12190-0

Emtage, L., Gu, G., Hartwieg, E., Chalfie, M., 2004. Extracellular Proteins Organize the Mechanosensory Channel Complex in C. elegans Touch Receptor Neurons. Neuron 44, 795–807. https://doi.org/10.1016/j.neuron.2004.11.010

Fehlauer, H., Nekimken, A.L., Kim, A.A., Pruitt, B.L., Goodman, M.B., Krieg, M., 2018. Using a Microfluidics Device for Mechanical Stimulation and High Resolution Imaging of C. elegans. JoVE J. Vis. Exp. e56530–e56530. https://doi.org/10.3791/56530

Geffeney, S.L., Cueva, J.G., Glauser, D.A., Doll, J.C., Lee, T.H.-C., Montoya, M., Karania, S., Garakani, A.M., Pruitt, B.L., Goodman, M.B., 2011. DEG/ENaC but Not TRP Channels Are the Major Mechanoelectrical Transduction Channels in a C. elegans Nociceptor. Neuron 71, 845–857. https://doi.org/10.1016/j.neuron.2011.06.038

Goodman, M.B., Hall, D.H., Avery, L., Lockery, S.R., 1998. Active Currents Regulate Sensitivity and Dynamic Range in C. elegans Neurons. Neuron 20, 763–772. https://doi.org/10.1016/S0896-6273(00)81014-4

Kang, L., Gao, J., Schafer, W.R., Xie, Z., Xu, X.Z.S., 2010. C. elegans TRP Family Protein TRP-4 Is a Pore-Forming Subunit of a Native Mechanotransduction Channel. Neuron 67, 381–391. https://doi.org/10.1016/j.neuron.2010.06.032

Katta, S., Krieg, M., Goodman, M.B., 2015. Feeling Force: Physical and Physiological Principles Enabling Sensory Mechanotransduction. Annu. Rev. Cell Dev. Biol. 31, 347–371. https://doi.org/10.1146/annurev-cellbio-100913-013426

Krieg, M., Stühmer, J., Cueva, J.G., Fetter, R., Spilker, K., Cremers, D., Shen, K., Dunn, A.R., Goodman, M.B., 2017. Genetic defects in β-spectrin and tau sensitize C. elegans axons to movement-induced damage via torque-tension coupling. eLife 6. https://doi.org/10.7554/eLife.20172

Lesniak, D.R., Gerling, G.J., 2009. Predicting SA-I mechanoreceptor spike times with a skin-neuron model. Math. Biosci. 220, 15–23. https://doi.org/10.1016/j.mbs.2009.03.007

Lewis, A.H., Cui, A.F., McDonald, M.F., Grandl, J., 2017. Transduction of Repetitive Mechanical Stimuli by Piezo1 and Piezo2 Ion Channels. Cell Rep. 19, 2572–2585. https://doi.org/10.1016/j.celrep.2017.05.079

Loewenstein, W.R., Mendelson, M., 1965. Components of receptor adaptation in a Pacinian corpuscle. J. Physiol. 177, 377–397. https://doi.org/10.1113/jphysiol.1965.sp007598

Loewenstein, W.R., Skalak, R., 1966. Mechanical transmission in a Pacinian corpuscle. An analysis and a theory. J. Physiol. 182, 346–378. https://doi.org/10.1113/jphysiol.1966.sp007827

Mendelson, M., Loewenstein, W.R., 1964. Mechanisms of Receptor Adaptation. Science 144, 554–555. https://doi.org/10.1126/science.144.3618.554

Nekimken, A.L., Mazzochette, E.A., Goodman, M.B., Pruitt, B.L., 2017. Forces applied during classical touch assays for Caenorhabditis elegans. PLOS ONE 12, e0178080. https://doi.org/10.1371/journal.pone.0178080

O'Hagan, R., Chalfie, M., Goodman, M.B., 2005. The MEC-4 DEG/ENaC channel of Caenorhabditis elegans touch receptor neurons transduces mechanical signals. Nat. Neurosci. 8, 43–50. https://doi.org/10.1038/nn1362

Peng, A.W., Ricci, A.J., 2016. Glass Probe Stimulation of Hair Cell Stereocilia, in: Sokolowski, B. (Ed.), Auditory and Vestibular Research: Methods and Protocols. Springer New York, New York, NY, pp. 487–500. https://doi.org/10.1007/978-1-4939-3615-1_27

Petzold, B.C., Park, S.-J., Mazzochette, E.A., Goodman, M.B., Pruitt, B.L., 2013. MEMS-based force-clamp analysis of the role of body stiffness in C. elegans touch sensation. Integr. Biol. 5, 853–864. https://doi.org/10.1039/C3IB20293C

Quindlen, J.C., Lai, V.K., Barocas, V.H., 2015. Multiscale Mechanical Model of the Pacinian Corpuscle Shows Depth and Anisotropy Contribute to the Receptor's Characteristic Response to Indentation. PLOS Comput. Biol. 11, e1004370. https://doi.org/10.1371/journal.pcbi.1004370

Quindlen-Hotek, J.C., Barocas, V.H., 2018. A finite-element model of mechanosensation by a Pacinian corpuscle cluster in human skin. Biomech. Model. Mechanobiol. 17, 1053–1067. https://doi.org/10.1007/s10237-018-1011-1

Rall, W., 1967. Distinguishing theoretical synaptic potentials computed for different soma-dendritic distributions of synaptic input. J. Neurophysiol. 30, 1138–1168. https://doi.org/10.1152/jn.1967.30.5.1138

Sanzeni, A., Katta, S., Petzold, B., Pruitt, B.L., Goodman, M.B., Vergassola, M., 2018. Tissue mechanics and somatosensory neural responses govern touch sensation in C. elegans. bioRxiv 471904. https://doi.org/10.1101/471904

Suzuki, H., Kerr, R., Bianchi, L., Frøkjær-Jensen, C., Slone, D., Xue, J., Gerstbrein, B., Driscoll, M., Schafer, W.R., 2003. In Vivo Imaging of C. elegans Mechanosensory Neurons Demonstrates a Specific Role for the MEC-4 Channel in the Process of Gentle Touch Sensation. Neuron 39, 1005–1017. https://doi.org/10.1016/j.neuron.2003.08.015

Thein, M.C., McCormack, G., Winter, A.D., Johnstone, I.L., Shoemaker, C.B., Page, A.P., 2003. Caenorhabditis elegans exoskeleton collagen COL-19: An adult-specific marker for collagen modification and assembly, and the analysis of organismal morphology. Dev. Dyn. 226, 523–539. https://doi.org/10.1002/dvdy.10259

Abbreviations

MeT: mechano-electrical transduction

MRC: mechanoreceptor current

TRN: touch receptor neuron

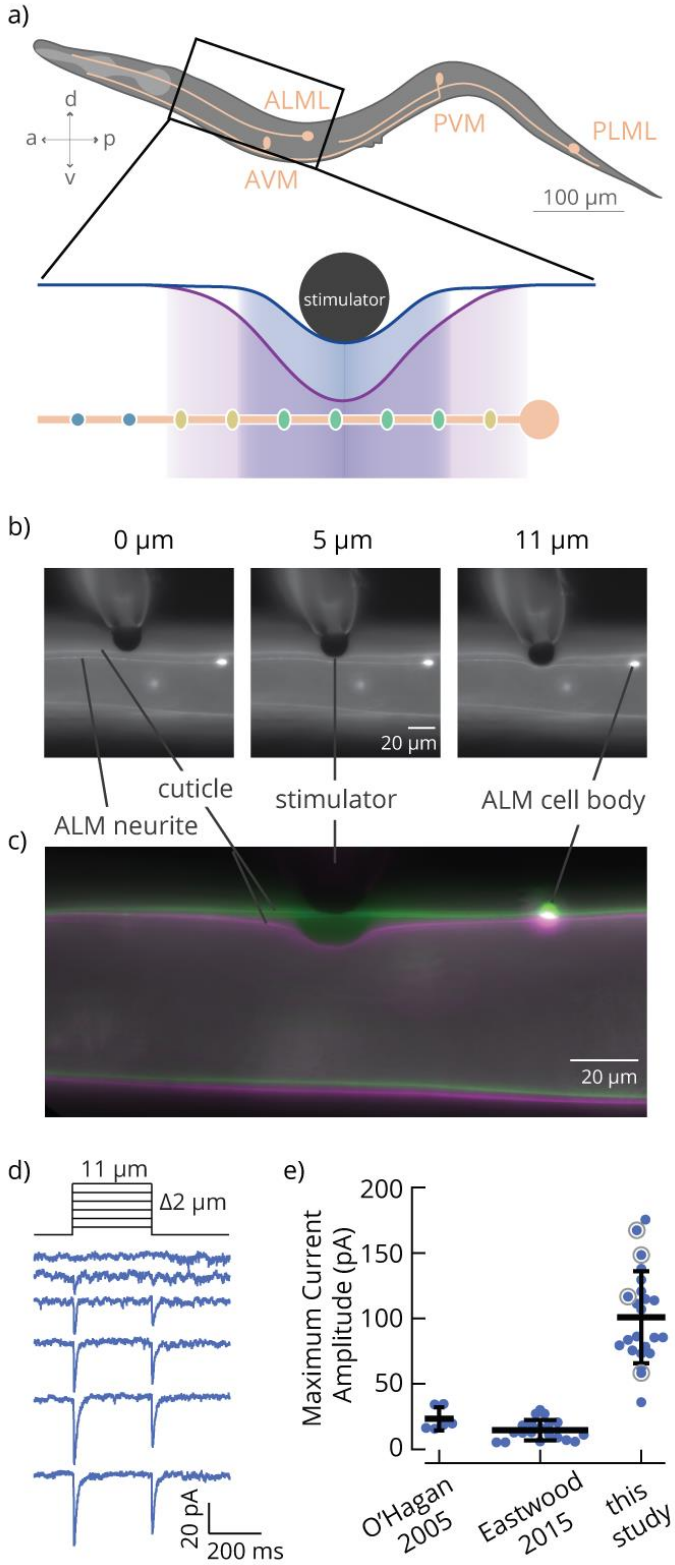

Figure 1. Increasing indentation increases the extent of cuticle deformation.

(A) Illustration of the ALM neuron and the hypothesized mechanism of channel recruitment. A small indentation (blue line) deforms the cuticle slightly and creates strain in the tissue and the neurite (blue shading) that reaches a small number of channels (green ovals). A larger indentation (purple line) deforms the cuticle at a greater distance and opens channels further from the stimulus (yellow ovals). Some channels remain outside the range of strain induced by even large cuticle deformation (blue circles). **(B)** A 22 µm black polyethylene bead indents an intact GN865 animal at different depths. Deformation is visible in the cuticle and the ALM neuron, which are both labeled with GFP. **(C)** An overlay shows the extent of cuticle deformation with a 22 µm bead before (green) and during (magenta) an 11 µm stimulus in a different GN865 animal, with ALM outside the plane of focus. **(D)** Representative traces from a set of indenting stimuli show increasing responses at the onset and offset. **(E)** The peak current measured in this study (10 µm displacement) is larger than currents elicited by saturating stimuli using published methods (Eastwood et al. (2015), 1.7 µN force; O'Hagan et al. (2005), > 1 µN force). Error bars represent mean ± standard deviation. Gray circles indicate recordings for which curves are shown in Fig. 2 A and B.

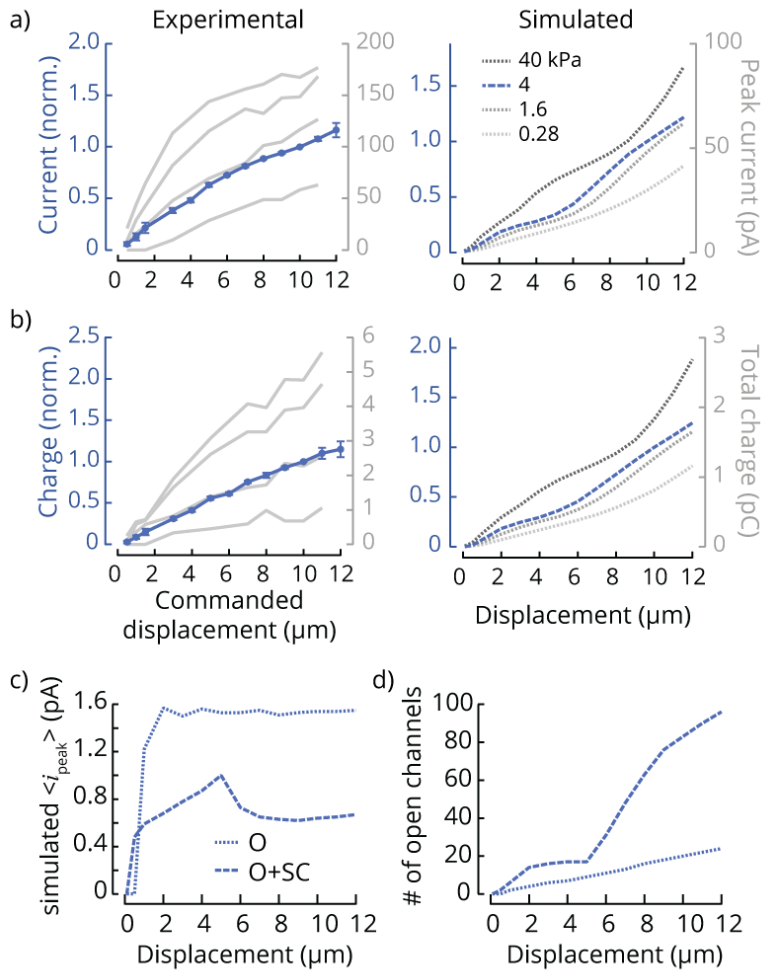

Figure 2. MRC sensitivity depends on body mechanics and channel recruitment.

(A, B) Left: experimentally measured peak MRC amplitude **(A)** or total charge carried by MRC **(B)** vs. displacement. For average responses (blue), we normalized each recording to the peak current or total charge at 10 µm, shown in Fig. 1 E. Error bars show mean ± s.e.m for n = 22 worms. Variations between experimental dissections are evident in four individual curves (gray) from the recordings indicated in Fig. 1 E. Right: simulated peak MRC **(A)** or total charge **(B)** vs. displacement given different internal pressures (mimicking variation in experimental dissections). **(C)** The mean peak current per activated channel in simulations increases with small displacements but remains constant at larger displacements. A threshold of 0.5*imax reflects the open probability of channels in the open (O) state (solid line) while a threshold of 0.1*imax includes both O and sub-conducting (SC) channels (dotted line). **(D)** The number of simulated channels in the O or SC state increases continuously with displacement and does not saturate within this range of displacements. Calculated using the same thresholds as used in panel C.

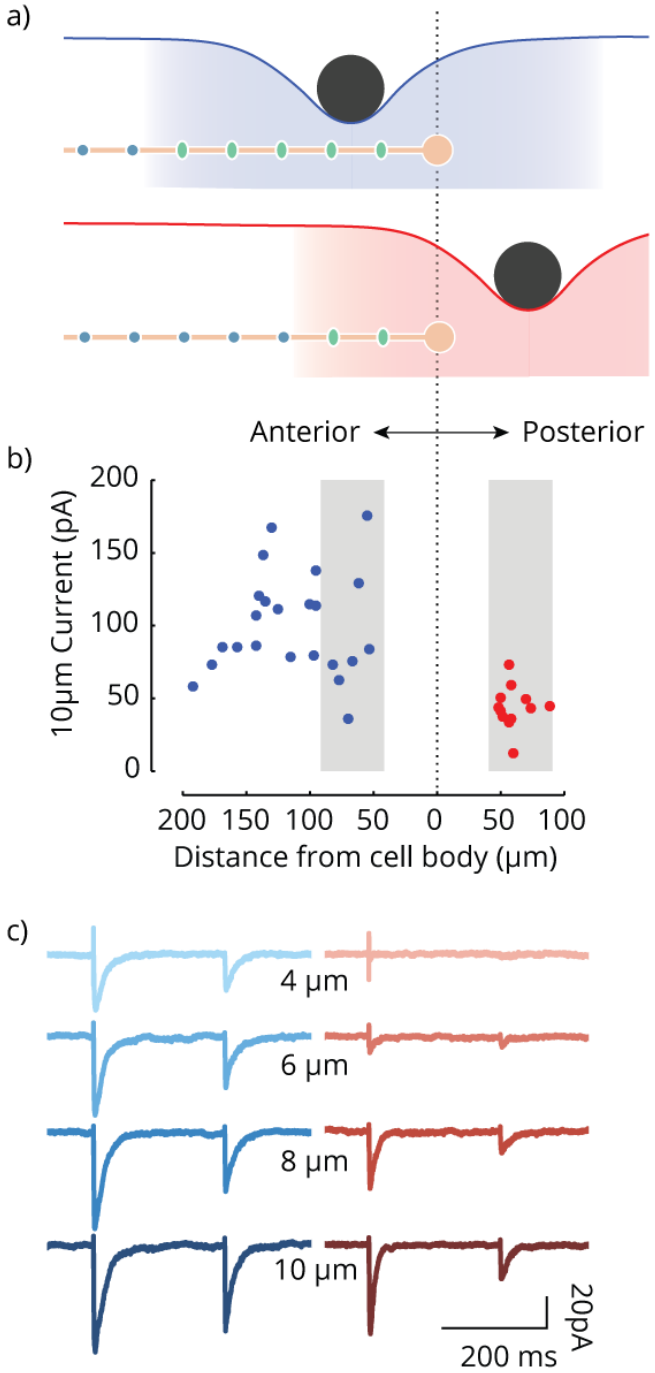

Figure 3. MRCs are evoked by indentations distant from the channels.

(A) Diagram illustrating how positioning a stimulus anterior to the ALM cell body (top) is predicted to activate more channels (green ovals) than positioning the same stimulus posterior to the cell body (bottom). **(B)** MRC responses to a 10 µm step are smaller when the stimulus is posterior (red) to the cell body than when it is anterior (blue). Each dot represents a separate recording. We corrected anterior currents for space-clamp error. Gray shading indicates recordings with a stimulus distance between 40 and 90 µm from the cell body. **(C)** Representative traces are shown from whole-cell recordings with anterior (left, 53 µm distance) or posterior (right, 58 µm distance) stimulation.

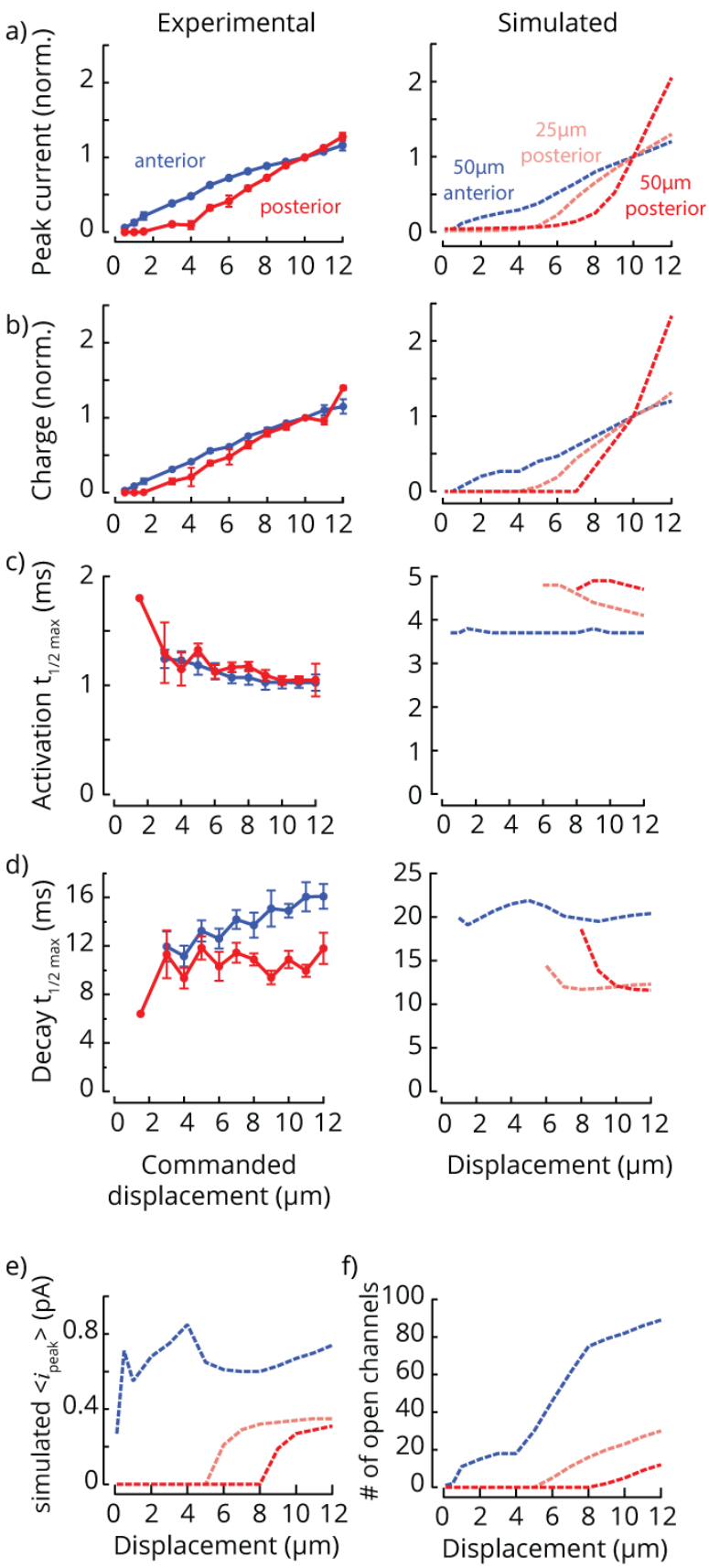

Figure 4. Stimulating from a distance requires greater indentation to evoke MRCs.

(A) Left: Experimentally measured peak current for stimulation posterior to the cell body (red) requires larger stimulus displacement than anterior stimulation (blue). Each recording was normalized to the current or charge at 10 µm. Error bars show mean ± s.e.m for n = 22 worms (anterior) or n = 12 worms (posterior). Anterior current is the same as shown in Fig. 2 A. Right: Simulated peak currents for stimuli located 25 µm (pink) or 50 µm posterior (red) to the cell body show the same rightward shift compared to a stimulus 50 µm anterior (blue). **(B)** The experimental relationship between total charge and displacement (left panel) does not shift to the right with posterior stimulation as much as the simulation (right panel) predicts. **(C, D)** Here we show activation time to half-maximal current from the stimulus start as well as decay time to half-maximal current from the peak. Experimental results were limited to recordings with a stimulus distance <90 µm (gray shading in Fig. 3 B). n = 7 (anterior) or n = 11 (posterior). Right panels show simulated results. **(E, F)** Moving the stimulus further posterior decreased the mean peak current per active channel **(E)** and increased the displacement required to open even one channel **(F).** The threshold of 0.1*imax for active channels includes both open and sub-conducting channels.

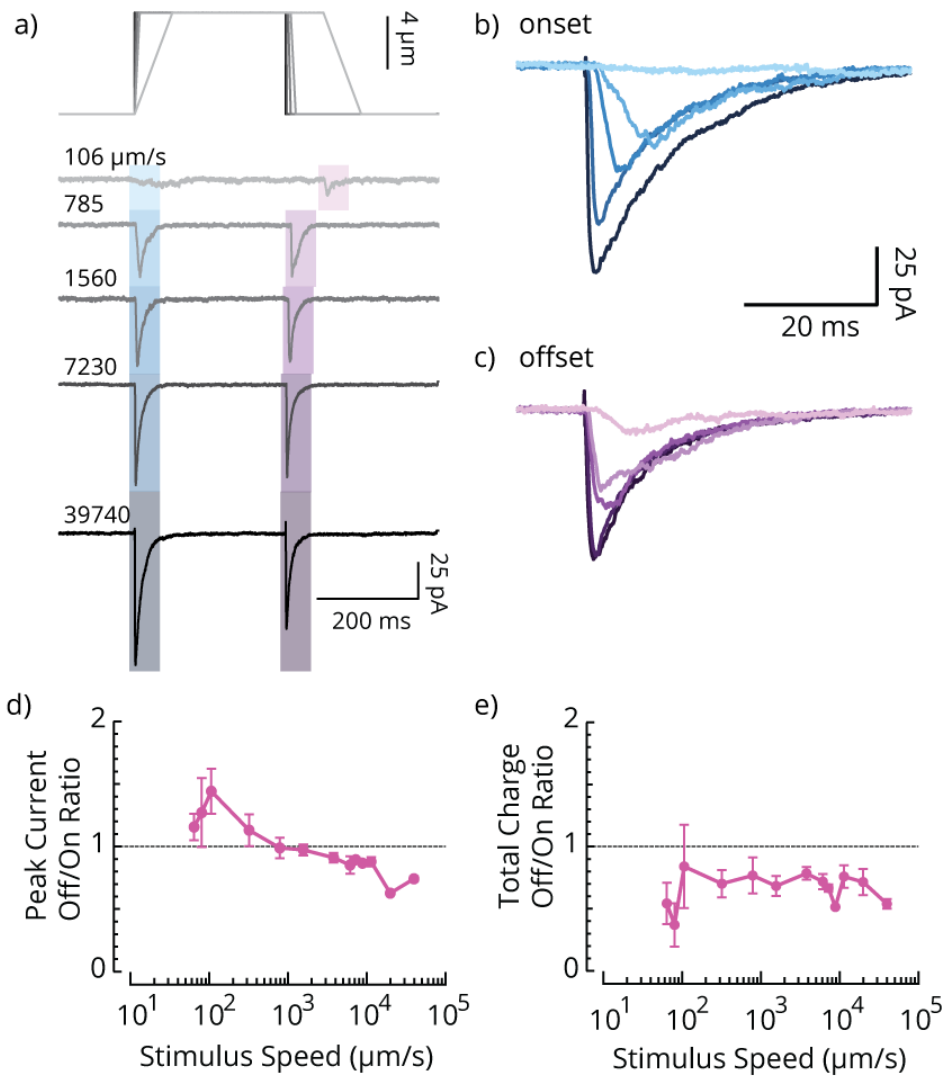

Figure 5. Stimulus speed increases MRC amplitude and hastens activation.

(A) Representative traces show that MRC responses to trapezoidal stimulation anterior to the cell body increase with stimulus speed. **(B, C)** Expansion of MRCs at the onset **(B)** and offset **(C)** of a stimulus. Currents at the onset are larger at fast speeds, but smaller and slower to activate at low speeds. **(D, E)** Ratio of 'off' response relative to 'on' response amplitudes, measured as either peak current **(D)** or total charge **(E)** for n = 6 worms with 2-9 technical replicates per recording. At slow speeds, 'off' peak currents are larger; at fast speeds, 'on' currents are larger. The total charge carried by 'off' responses, however, is consistently smaller than that of 'on' responses at all stimulus speeds.

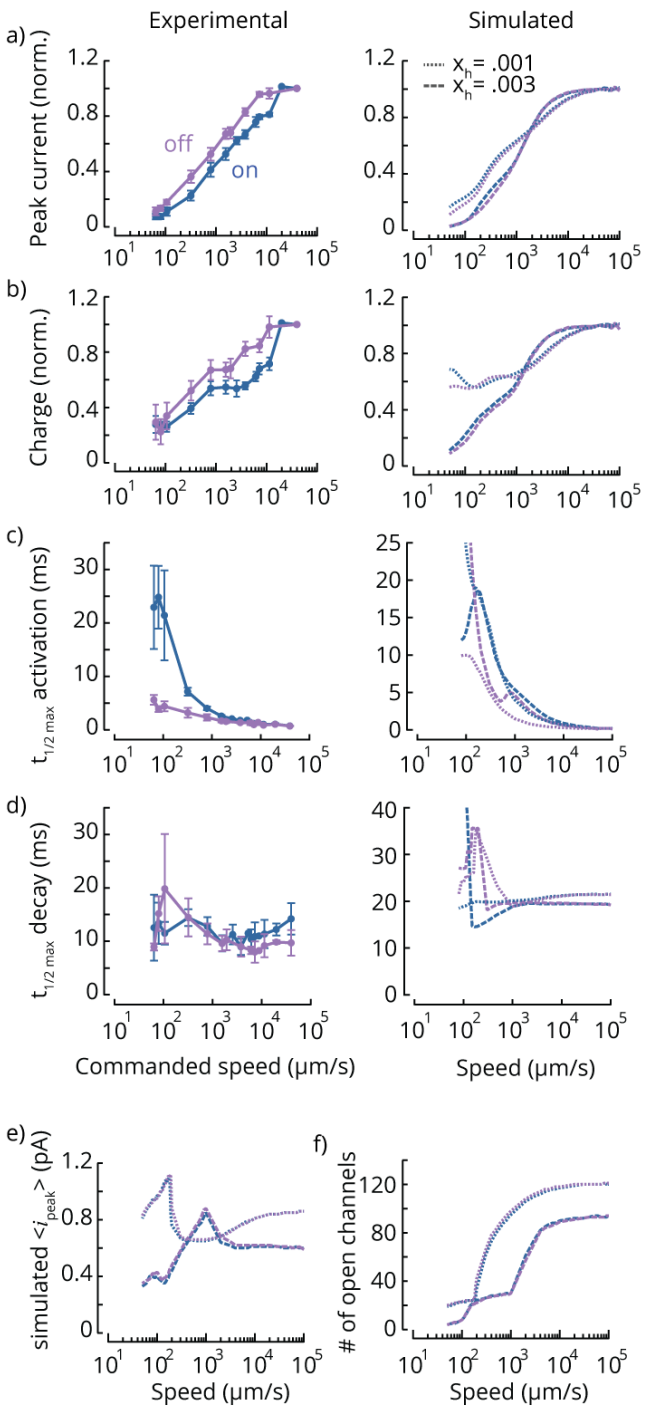

Figure 6. Synchrony in channel opening only partially explains 'on'/'off' asymmetry.

(A, B) Left: Both peak current **(A)** and total charge **(B)** show that the sensitivity of normalized 'off' responses (purple) to stimulus speed shifts left relative to 'on' responses (blue). Error bars show mean ± s.e.m. Right: Simulated speed sensitivity is similar for 'on' and 'off' responses, and the current saturates at high speeds. Data were normalized to the response to a step (39,740 µm/s experimentally or 40,000 µm/s for simulations). n = 6 recordings. Simulations were performed with the default force required to activate a channel x_h = 0.003 (dashed) or a smaller x_h = 0.001 (dotted). **(C)** 'On' currents activate more slowly than 'off' currents at slow speeds; simulated data (right) show a similar trend at the range of speeds tested experimentally. **(D)** The MRC decay rate is similar for both 'on' and 'off' currents; simulated data (right) show similar behavior at high speeds. **(E)** Mean peak single-channel current from the simulation increases initially with speed, and then plateaus. **(F)** The number of channels opened increases with speed, but saturates at high speeds. The same thresholds are used as E.

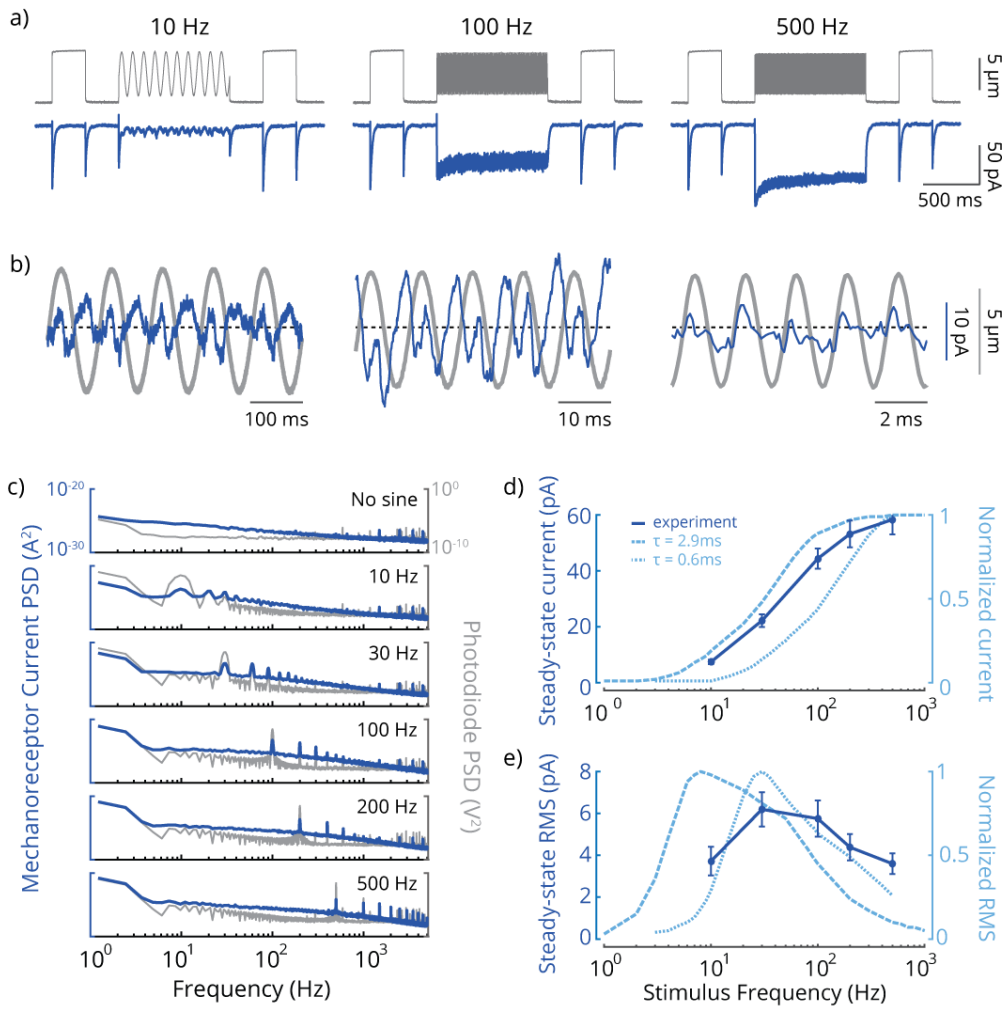

Figure 7. MRCs evoked by sinusoidal stimuli have complex temporal dynamics.

(A) Representative traces of MRCs (blue) evoked by sinusoidal stimuli delivered anterior to the cell body. Dotted line indicates baseline current. Gray traces show photodiode-based measurements of actual bead motion. Each trace is a mean of six repetitions from a single recording. Individual sweeps show a similar behavior. We used flanking square pulses to assess the recording quality. **(B)** Expanded responses from panel A (blue) overlaid on the photodiode measurement of bead motion (gray) show responses at roughly 2x the stimulus frequency. The dashed line indicates steady-state current. **(C)** The power spectrum of mechanoreceptor responses during the sine (blue) shows similarly sized peaks at 1x and 2x the stimulus frequency, while the power spectrum of the photodiode measurement shows a large peak at the stimulus frequency and smaller peaks at the harmonics. **(D)** Experimental steady-state current over the last 100 ms of the sinusoid (dark, solid) shifts to higher frequencies than simulated steady-state current normalized to the maximum (light, dashed). Shortening the relaxation time τ of the elastic filament in the model from the previously used value of 2.9 ms to 0.6 ms also shifts the prediction to higher frequencies (light, dotted). Error bars shown mean ± s.e.m. for n = 7 worms. **(E)** The amplitude of sinusoidal current measured as RMS around the steady-state mean over the last 100 ms of the sinusoid (dark, solid) and the RMS of simulated current normalized to the maximum (light, dashed) both show band-pass behavior. However, the experimental data shifts to higher frequencies than the simulation. Shortening the filament τ shifts the peak to higher frequencies (light, dotted).

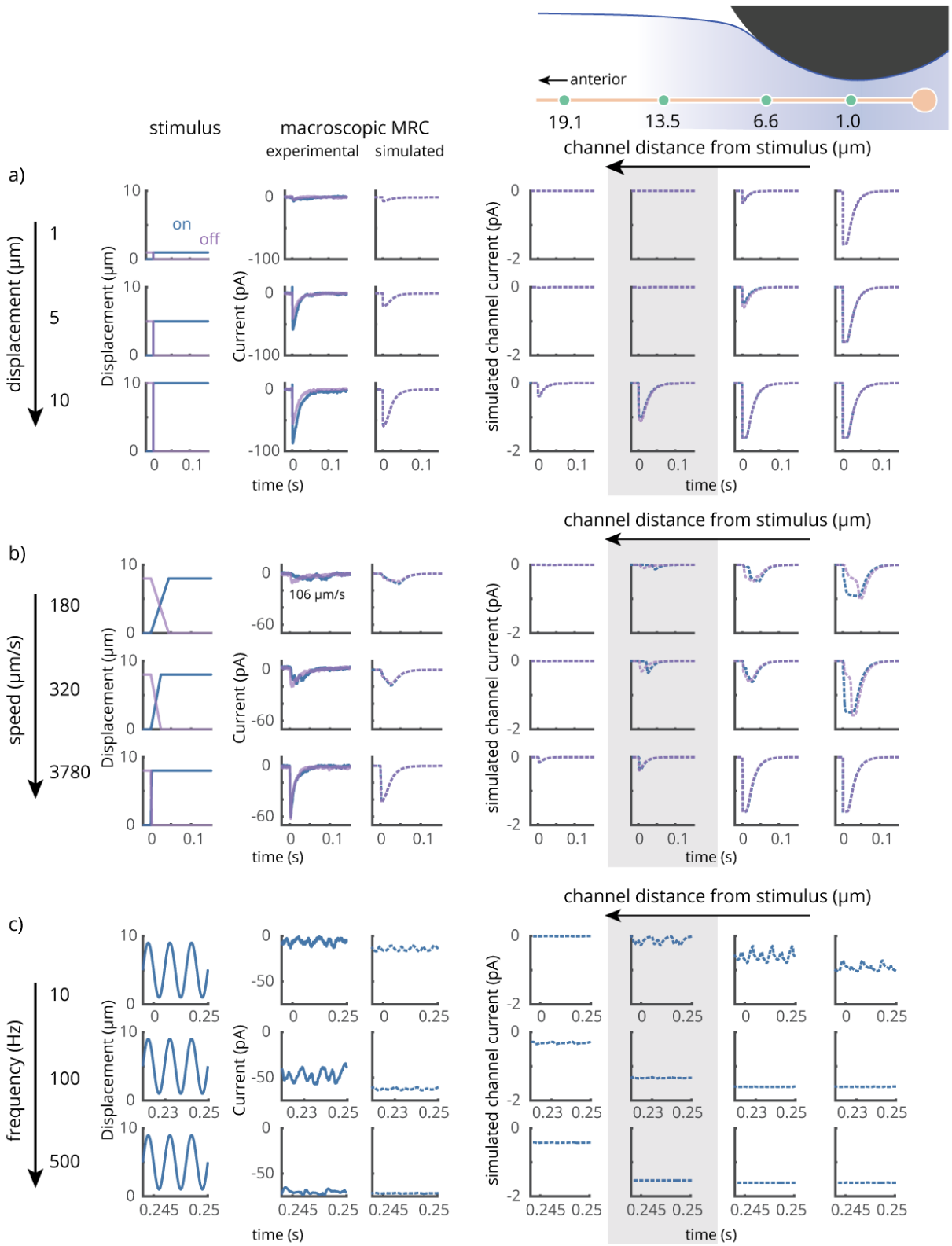
anterior
19.1
13.5
6.6
1.0
stimulus
macroscopic MRC
experimental
simulated
channel distance from stimulus (μm)
a)
displacement (μm)
1
5
10
on
off
Displacement (μm)
Current (pA)
simulated channel current (pA)
time (s)
b)
speed (μm/s)
180
320
3780
106 μm/s
c)
frequency (Hz)
10
100
500

Figure 8. Simulated single-channel responses depend on channel position and stimulus intensity.

The first three columns show overlaid example stimuli at the onset (blue) and offset (purple), representative traces of observed currents for the stimulus in each row, and simulated currents. The last four columns show simulated current through individual channels positioned either (left to right) 19.1, 13.5, 6.6, or 1 µm anterior to the stimulus in each row**. (A)** Increasing displacement evokes larger currents at the onset and offset by recruiting channels farther away from the stimulus. The highlighted channel located 13.5 µm from the stimulus does not open until the indentation is large. **(B)** Increasing speed evokes larger currents by increasing synchrony, increasing the probability of being open, and recruiting more distant channels. 'On' current through the highlighted channel has a higher latency at slow stimulus speeds, but matches the 'off' current at fast speeds. We measured the experimental current at 106 rather than 180 µm/s. **(C)** Increased frequency evokes larger but more consistent steady-state currents by recruiting more distant channels and increasing the open probability. We obtained experimental responses at various time points to match the stimulus phase, but we took all responses during the steady-state period of a 1 s sine response. We captured simulated traces at the end of a 500 ms sine centered at t = 0.

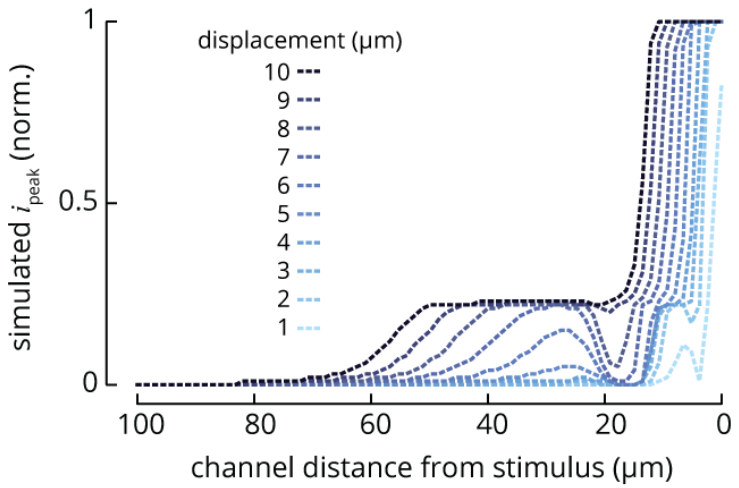

Figure S1. Individual channel responses depend on both channel distance and stimulus size.

The peak current through individual channels (normalized to the single-channel current i = 1.6 pA) in response to a step stimulus is highest for channels near the point of stimulation. At further distances, the current reflects the non-linearity of the strain field and increasing likelihood of the channel being in a sub-conducting rather than a fully open state.